Unusual x-ray excited luminescence spectra of NiO suggest self-trapping of the *d*-*d* charge-transfer exciton

V. I. Sokolov,[1] V. A. Pustovarov,[2] V. N. Churmanov,[2] V. Yu. Ivanov,[2] N. B. Gruzdev,[1] P. S. Sokolov,[3] A. N. Baranov,[3] and A. S. Moskvin[4]

[1]*Institute of Metal Physics, Ural Division, RAS, S. Kovalevskaya street 18, 620990 Ekaterinburg, Russia*

[2]*Ural Federal University, Mira street 19, 620002 Ekaterinburg, Russia*

[3]*Department of Chemistry, Moscow State University, 119991 Moscow, Russia*

[4]*Department of Theoretical Physics, Institute of Natural Sciences, Ural Federal University, Lenin street 51, 620083 Ekaterinburg, Russia*

(Received 20 January 2012; revised manuscript received 2 July 2012; published 20 September 2012)

Luminescence spectra of NiO have been investigated under vacuum ultraviolet (VUV) and soft x-ray (XUV) excitation (DESY, Hamburg). Photoluminescence (PL) spectra show broad emission violet and green bands centered at about 3.2 and 2.6 eV, respectively. The PL excitation (PLE) spectral evolution and lifetime measurements reveal that the two mechanisms with short and long decay times, attributed to the $d(e_g)$-$d(e_g)$ and $p(\pi)$-d charge transfer (CT) transitions in the range 4–6 eV, respectively, are responsible for the observed emissions. The XUV excitation makes it possible to avoid the predominant role of the surface effects in luminescence and reveals a bulk violet luminescence with a puzzling well-isolated doublet of very narrow lines. These lines with close energies near 3.3 eV are attributed to recombination transitions in the self-trapped d-d CT excitons formed by the coupled Jahn-Teller Ni^{+} and Ni^{3+} centers. The conclusion is supported by a comparative analysis of the luminescence spectra for NiO and solid solution $Ni_xZn_{1-x}O$ and by a comprehensive cluster model assignment of different p-d and d-d CT transitions and their relaxation channels. Our paper shows that the time-resolved luminescence measurements provide an instructive tool for the elucidation of the p-d and d-d CT excitations and their relaxation in 3d oxides.

DOI: 10.1103/PhysRevB.86.115128 PACS number(s): 71.35.−y, 78.47.jd, 71.10.Li, 78.20.Bh

I. INTRODUCTION

Explaining the electronic properties of transition-metal monoxides is one of the long-standing problems in condensed-matter physics. Nickel monoxide (NiO), with its rather simple rock-salt-type structure, a large insulating gap, and an antiferromagnetic ordering temperature of $T_N = 523$ K, has been attracting many physicists as a prototype oxide for this problem.[1] This strongly correlated electron material plays an important role in clarifying the electronic structure and understanding the physical properties of 3d compounds. The recent discoveries of a giant low-frequency dielectric constant, a bistable resistance switching, and other unconventional properties[2] have led to a major resurgence of interest in NiO.

However, despite several decades of studies[1] there is still no consensus on the detailed electronic structure of NiO, including the energy gap E_g, whose values are reported as being from 3.7 eV (Ref. 3) to 5 eV.[4] The conventional band theories which stress the delocalized nature of electrons cannot explain this large gap and predict NiO to be metallic. NiO has long been viewed as a prototype "Mott insulator,"[1] with the gap formed by intersite d-d charge transfer (CT) transitions; however, this view was later replaced by that of a "CT insulator"[5] with the gap formed by p-d CT transitions. The most recent resonant inelastic x-ray scattering (RIXS) and optical reflectivity measurements[4] showed that the CT band peaked near 4–5 eV reveals a discernible q dispersion of its energy typical of the Mott-Hubbard d-d CT transitions, while an intense CT band at a higher-energy peaked near 7–8 eV reveals only an intensity dispersion without any visible dispersion of the energy, which is typical for the intracenter p-d CT transitions. Nevertheless, to date we have no comprehensive assignment of different spectral features in NiO to p-d or d-d CT transitions.

Charge carriers and excitons photogenerated in a crystal with a strong electron-lattice interaction are known to relax to self-trapped states, causing a local lattice deformation and forming luminescence centers.[6] Some quite basic questions concerning the self-trapped exciton remain unresolved, even in the alkali halides, which are traditionally regarded as prototype insulating materials in which the microscopic features of the self-trapping processes have been studied most extensively. At the same time, luminescence spectroscopy can give profound insight into the electronic structure, electron-hole excitations, and their relaxation in the lattice.

The optical emission properties of NiO have been scarcely investigated. Different measurements performed with UV excitation below and near the optical gap[7–9] point to a broad luminescence band in the region 2–3.5 eV. The temperature behavior indicates that the broad photoluminescence (PL) spectra consist of several components with a relative intensity dependent on the temperature and excitation energy. The low-energy excitation ($E_{exc} \approx 2.4$ eV) below the charge-transfer gap stimulates a photoemission in a single-crystal NiO with two maxima, one at 1.5–1.6 eV and a larger one at 2.2–2.3 eV.[10] The green luminescence band with a maximum around 2.25 eV has been observed in nanoclustered NiO at $E_{exc} \leqslant 2.95$ eV.[8] The emission bands observed in the visible and near-infrared spectral ranges are usually attributed to Ni^{2+} intrasite or crystal-field d-d transitions (see, e.g., Ref. 11). In particular, the main green luminescence band peaked near 2.3 eV is attributed to a Stokes-shifted $^1T_{2g}(D) \rightarrow {}^3A_{2g}(F)$ transition, while the low-energy band peaked near 1.5 eV is related to a $^1E_g(D) \rightarrow {}^3A_{2g}(F)$

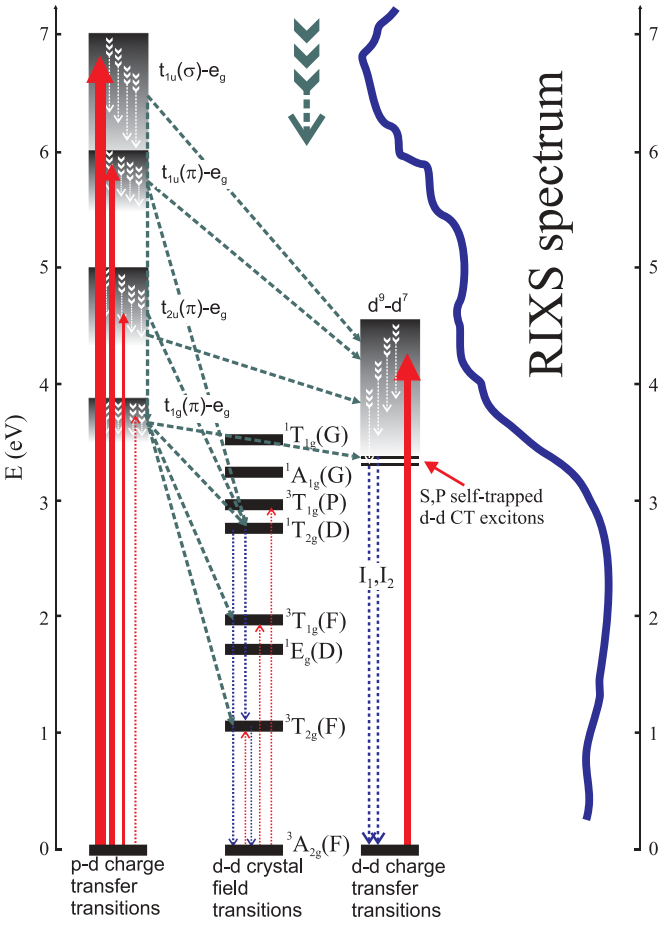

FIG. 1. (Color online) Spectra of the *d*-*d* and *p*-*d* CT transitions and intracenter crystal-field *d*-*d* transitions in NiO. Strong dipole-allowed σ-σ *d*-*d* and *p*-*d* CT transitions are shown by thick solid up arrows, weak dipole-allowed π-σ *p*-*d* transitions are shown by thin solid up arrows, and weak dipole-forbidden low-energy transitions are shown by thin dashed up arrows. Dashed down arrows point to different electron-hole relaxation channels, and dotted down arrows point to PL transitions. The spectrum of the crystal field *d*-*d* transitions is reproduced from Ref. 12. The right-hand side reproduces a fragment of the RIXS spectra for NiO.[13]

transition[10] (see Fig. 1 for the spectrum of the crystal-field *d*-*d* transitions[12]). However, the photoluminescence spectra of bulk single crystals and ceramics of NiO under 3.81 eV photoexcitation[9] suggestive the band gap excitation have revealed in addition to the green band, a more intensive broad violet PL band with a maximum around 3 eV. The band was related to a *p*-*d* charge transfer. A radiative recombination of carriers in powdered pellets of NiO under the UV excitation with $E_{\rm exc} = 4.43$ eV (280 nm) higher than the CT gap consists at 10 K of a broad intense band peaked at 2.8 eV with a shoulder centered at about 3.2 eV.[7] It is clearly appreciated that the 2.8-eV emission band decreases with increasing temperature, while the 3.2-eV band follows a strictly opposite trend and becomes the dominant emission at about 150 K. Furthermore, the 3.2-eV band reveals a two-peak structure clearly visible at elevated temperatures. Different kinetic properties, seemingly a different temperature behavior,[7] point to different relaxation channels governing the green and violet luminescences.

The comparison of the PL spectra with the cathodoluminescence (CL) spectra of the same samples[7] reveals differences in the relative intensity of the excited emissions. The 2.8- and 3.2-eV PL bands appear in the CL spectra as shoulders of a main broad green 2.4-eV emission band. However, for the NiO samples annealed in vacuum both the 2.4- and 3.2-eV bands have a comparable spectral weight and a clearly visible multipeak structure. The green 2.4-eV band is visible in the time-resolved PL spectra recorded at 10 K for different delay times.[7] At variance with Ref. 9 the PL and CL emission bands observed in this work[7] were attributed to the crystal-field *d*-*d* transitions. However, such an attribution seems to be questionable since the candidate initial excited $3d^8$ states for the proper radiative transition, $^1T_{1g}(G)$ or $^1A_{1g}(G)$, can nonradiatively relax to the close low-lying terms, $^3T_{1g}(P)$ and $^1T_{2g}(D)$ (see Fig. 1). Thus, one may conclude that the nature of the pregap violet luminescence in NiO remains unclear. The elucidation of the problem was one of the stimulating points for our research, which implied the high-energy excitation ($E_{\rm exc} > E_g$) of the luminescence. To the best of our knowledge, the PL excitation (PLE) has been previously restricted by $E_{\rm exc} = 4.43$ eV,[7] with no inspection of the PL photoexcitation over the CT band, though such a study could be an instructive tool to elucidate the mechanism of the CT transitions and the spectral selectivity of the PL.

It is worth noting that all the studies of the PL in NiO point to a specific role of different defects and the surface structures with a low crystal symmetry. These may create in-gap states acting as luminescence centers displaying a broad luminescence band. Indeed, the most effective absorption of photons with the energy $\hbar\omega \geqslant E_g$ in NiO, given an absorption coefficient $\geqslant 0.5 \times 10^6$ cm^{-1} (Refs. 12, 14, and 15), occurs in a thin ($\leqslant$20 nm) surface layer with a more or less distorted symmetry and an enhanced defect concentration. In other words, the UV photoexcitation in NiO cannot stimulate the bulk luminescence, mirroring the fundamental material properties. These issues also motivated our studies of the photoluminescence spectra in NiO under a high-energy excitation by making use of both the VUV and soft x-ray time-resolved PL excitation technique (DESY, Hamburg) that provided a profound insight into a genuine electronic structure and electron-hole transitions. We have observed an unconventional bulk luminescence with a puzzling well-isolated doublet of very narrow lines. These lines have close energies near 3.3 eV in both NiO and solid solution $Ni_xZn_{1-x}O$, with the rock-salt-type structure. The comprehensive analysis of the *p*-*d* and *d*-*d* CT transitions, their relaxation channels, and the luminescence spectra for NiO and solid solutions points to a recombination transition in the self-trapped *nnn* Ni^+-Ni^{3+} *d*-*d* CT excitons as the only candidate source of an unconventional luminescence.

This paper is organized as follows. In the next section, we describe the samples of NiO and solid solution $Ni_xZn_{1-x}O$ with the rock-salt-type structure and the experimental technique used. Then we report our main experimental results, the PL and PLE spectra under both the VUV and soft x-ray time-resolved excitations. In the first part of Sec. III, the results of the cluster model analysis of the *p*-*d* and *d*-*d* CT transitions in NiO are presented. Here we report our interpretation of the PLE spectra and give and overview of the literature data, which do support our attribution of different

CT transitions. The second part of Sec. III is devoted to a justification of the *d*-*d* CT origin of the unconventional x-ray excited violet luminescence observed in NiO and $Ni_xZn_{1-x}O$ samples. Section IV summarizes our work.

II. EXPERIMENTAL RESULTS

A. Sample characterization and experimental methods

The PL measurements were made on the commercially available samples of NiO and several solid solution $Ni_xZn_{1-x}O$ ($x = 0.2$, 0.3, and 0.6) with a rock-salt-type (rs) crystal structure that were synthesized. As a starting material we have used the commercially available powder of NiO (99%; Prolabo) with a green color and ZnO (99.99%; Alfa Aesar), which have been pressed into pellets under a pressure of about 1250 bars and placed into gold capsules. The quenching experiments at 7.7 GPa and 1000–1200 °C were performed using a toroid-type high-pressure apparatus. The details of the experimental technique and calibration are described elsewhere.[16] The electron microscopy analysis shows the samples to be dense poreless oxide ceramics with an rs cubic structure and a grain size of about 10–20 μm. The intensity of the color of the synthesized $Ni_xZn_{1-x}O$ solid solutions was reduced to light green upon increasing ZnO content.

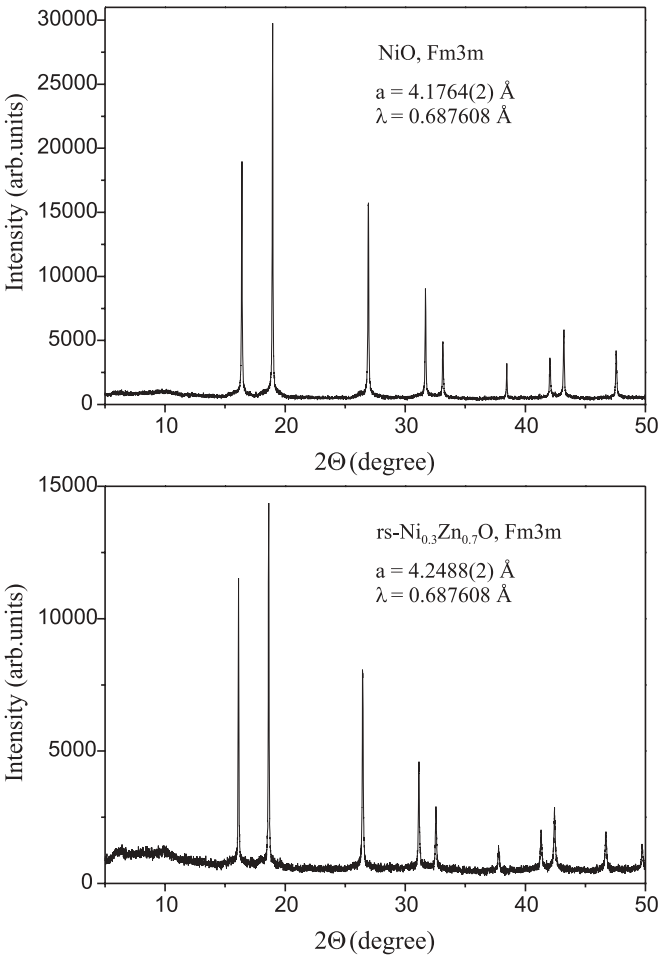

FIG. 2. The x-ray diffraction patterns of NiO and rs $Ni_{0.3}Zn_{0.7}O$ solid solutions recorded at room temperature.

Figures 2(a) and 2(b) show the results of the powder-diffraction measurements for NiO and rs $Ni_{0.3}Zn_{0.7}O$ solid solution synthesized by quenching at 7.7 GPa and 1470 K performed at beam line B2, DORIS III.[17] The 0.3-mm-diameter quartz capillaries were used as sample holders, and the measurements were performed at a wavelength of $\lambda = 0.687608$ Å in the Debye-Scherrer geometry with the on-site readable position-sensitive image-plate detector ($2\theta < 60°$, step size 0.004°).[18] It should be noted that the lattice parameters of rs $Ni_xZn_{1-x}O$ perfectly follow the linear concentration dependence (Vegard's law) from $a_{ZnO} = 4.280$ Å to $a_{NiO} = 4.176$ Å in the entire concentration range of the existence of the rs solid solutions.[16] The lattice parameter of NiO used in this work (4.176 Å) nicely agrees with that reported in the literature (see, e.g., Refs. 12 and 19). We have used x-ray absorption spectroscopy to identify the oxidation state of NiO and other solid solutions. The nickel *K*-edge extended x-ray absorption fine-structure measurements have been performed at beam line A1, DORIS III, with a Si (111) four-crystal monochromator. The x-ray absorption spectroscopy (XAS) spectra (not shown) were measured at room temperature in the fluorescence-detection mode using the passivated implanted planar silicon (PIPS) detector. The energy scale was calibrated with a Ni foil. The fluorescence yield was normalized to the intensity of the incoming beam. The oxidation state and coordination environment of Ni ions proved to be very similar in our NiO and rs $Ni_xZn_{1-x}O$ solid solutions. No trace of the Ni^{3+} was detected in our samples. The NiO and $Ni_{0.3}Zn_{0.7}O$ ceramic samples have been ground with a cellulose (carboxymethylcellulose, CMC) and then pressed into tablets to provide an enhancement of the luminescence intensity due to the effective surface enlargement (see below). It is worth noting that the procedure goes along with the partial oxidation/reduction processes and can positively influence the reduction of remnant Ni^{3+} ions undetectable by the XAS (less than 0.01 at. %).

The PL spectra have been excited by the synchrotron radiation (SR) with 1-ns pulses running at 96-ns intervals. The PL and PLE spectra were recorded in the 2–3.5 and 4–12 eV range, respectively.[20] The measurements of the PL spectra under the soft x-ray (XUV) excitation were made on a SUPERLUMI station [HASYLAB (DESY), Hamburg] using an ARC Spectra Pro-308i monochromator and a R6358P Hamamatsu photomultiplier. The time-resolved PL and PLE spectra, with the PL decay kinetics in the 1–80-ns interval, were measured in two time windows: fast, with a delay time $\delta t_1 = 0.6$ ns and a span of windows $\Delta t_1 = 2.3$ ns, and slow, with a delay time $\delta t_2 = 58$ ns, $\Delta t_2 = 14$ ns. The time-resolved PL spectra as well as the PL decay kinetics under the XUV excitation have been measured on a BW3 beam line by a VUV monochromator (Seya-Namioka scheme) equipped with a microchannel plate photomultiplier (MCP 1645, Hamamatsu). The parameters of time windows are as follows: $\delta t = 0.1$ ns, $\Delta t = 5.7$ ns. The temporal resolution of the whole detection system was 250 ps. The temporary interval between SR excitation pulses is equal to 96 ns.

B. PL spectra of NiO under VUV excitation

The photoluminescence spectra of the cellulose-free and the cellulose-coated NiO samples under the VUV excitation at

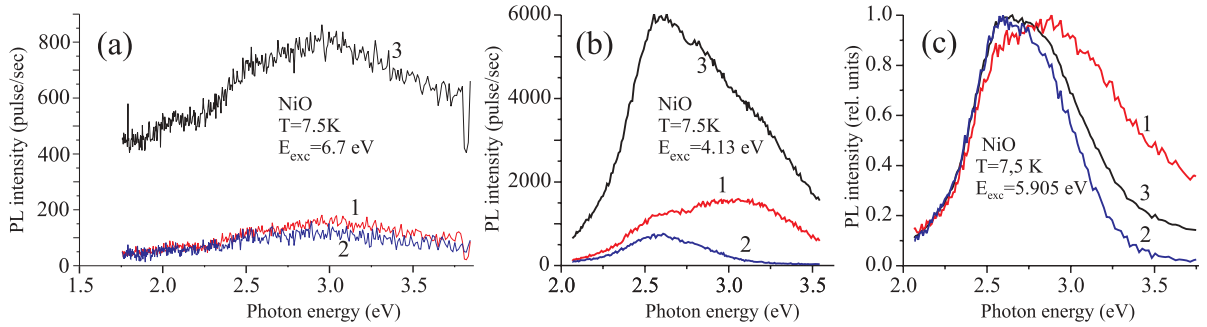

FIG. 3. (Color online) The time-resolved PL spectra (VUV excitation) of the (a) cellulose-free and (b) and (c) the cellulose-coated NiO samples: 1, a fast window; 2, a slow window; 3, a time-integrated spectrum. We make use of different units in (a) and (b) than in (c) to underline spectral features and strong differences of the PL intensities.

excitation energies $E_{\rm exc} > E_g$ and different registration regimes are presented in Fig. 3(a) and Figs. 3(b) and 3(c), respectively. In general, the spectra for both samples correspond to the literature data;[7,9] however, we should point out the spectacular growth of the PL intensities and the signal-to-noise ratio due to the cellulose coating of the NiO samples. Indeed, a simple comparison of the PL spectra in Figs. 3(a) and Fig. 3(b) shows that these quantities increase by almost one order of magnitude in the cellulose-coated sample compared with the cellulose-free NiO sample. Most likely, this is related to an effective sample surface enlargement. However, at variance with the cellulose-free sample the cellulose-coated NiO sample reveals a remarkably strong spectral sensitivity to the registration time. While the PL intensity of the cellulose-free sample has a smooth maximum near 3 eV which hardly depends on the registration time, the time-integrated PL spectrum for the cellulose-coated sample [Figs. 3(b) and 3(c), curve 3] has a distinct maximum near 2.6 eV (a green luminescence) and an extended high-energy tail which is more intense for the 4.13-eV excitation than for the 5.9-eV excitation. A significant difference in the PL spectra is revealed for fast and slow windows. The high-energy 5.9 eV excitation results in a sizable enhancement of PL in the high-energy range 3.0–3.5 eV for a fast window. However, the 4.13-eV excitation gives rise to a more pronounced selectivity effect with the intense maximum of the broad PL band shifted to 3.15 eV (a violet luminescence) for the fast window, while for the slow window one observes a broad PL band peaked near 2.6 eV (a green luminescence). The distinct registration time selectivity of green and violet emission bands points to different relaxation channels governing the green and violet luminescences. We see that the PL measurements in the fast time window provide an effective tool to inspect the nature of the violet luminescence.

Despite the low signal-to-noise ratio the PL excitation spectrum of the cellulose-free NiO sample at $E_{em} = 2.8$ eV shown in the top panel of Fig. 4 reveals several spectral maxima near 4, 5, 6, 9, and 12 eV. A more distinct PL excitation spectrum of the cellulose-coated NiO sample at $E_{em} = 2.75$ eV shown in the bottom panel of Fig. 4 reveals a significant effect of different observation conditions, particularly in the spectral range near 4 eV. It should be emphasized that the CT transition peaked near 4 eV working predominantly in the fast window is the most effective one in the excitation of the high-energy (violet) part of the PL spectrum. The time-integrated spectrum and the spectrum for a slow window present a broad maximum near 6 eV and a shoulder near 4.3 eV. For the fast window, the shoulder transforms into a narrow peak near 4 eV that is comparable in magnitude to a strong maximum near 6 eV. A sharp fall of the PLE intensity above 6 eV can be related mainly to the cellulose absorption that becomes noticeable just above 6 eV (Ref. 21; see Fig. 4, bottom panel). That is why

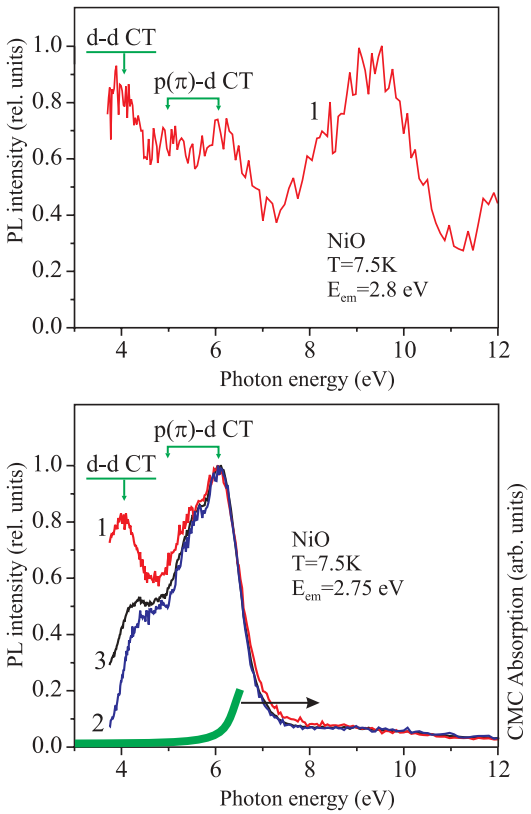

FIG. 4. (Color online) The time-resolved PLE spectra of (top) the cellulose-free and (bottom) the cellulose-coated NiO samples: 1, a fast window; 2, a slow window; 3, a time-integrated spectrum. Vertical arrows point to $d(e_g)$-$d(e_g)$ and $p(\pi)$-d ($t_{2u}(\pi) \rightarrow e_g$ and $t_{1u}(\pi) \rightarrow e_g$) CT transitions, which are the most effective in the PL excitation given $E_{\rm exc} < 7$ eV. The solid curve in the bottom panel shows the absorption for the cellulose reproduced from Ref. 21.

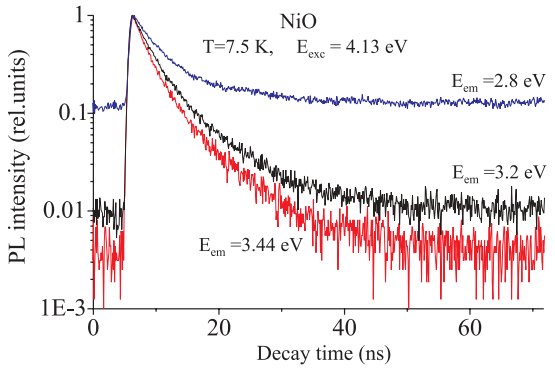

FIG. 5. (Color online) PL decay kinetics (VUV excitation) of NiO.

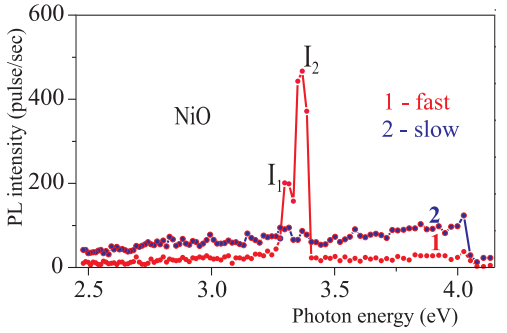

FIG. 6. (Color online) Survey luminescence spectra of the NiO sample under XUV excitation with energy $E_{exc} = 130$ eV at T = 7.2 K [fast (1) and slow (2) windows, spectral resolution of 10 meV].

we cannot reveal the 9- and 12-eV PLE spectral features that are distinctly visible for the cellulose-free NiO sample.

Interestingly, the PLE spectrum correlates with the reflectance,[22] electroreflectance,[23] and the RIXS[13] spectra of NiO in the spectral range 4–6 eV usually related to different CT transitions. According to Powell and Spicer,[22] the high-energy 9- and 12-eV PLE spectral features could be related to Ni^{2+} on-site $3d$-$4p$ or O $2p$ (t_{1u})–Ni $4s$ CT transitions.

The PL decay kinetics for the cellulose-coated NiO sample are shown in Fig. 5 for $E_{exc} = 4.13$ eV and different emission energies. The decay curves were approximated by a sum of two exponentials and a pedestal which describes a slow microsecond decay: $I(t) = y_0 + y_1 \exp(-t/\tau_1) + y_2 \exp(-t/\tau_2)$, where $\tau_1 = 3.4$ ns, $\tau_2 = 14.6$ ns, $y_0 = 0.11$ ($E_{em} = 2.8$ eV); $\tau_1 = 2.7$ ns, $\tau_2 = 8.2$ ns, $y_0 = 0.01$ ($E_{em} = 3.2$ eV); and $\tau_1 = 2.3$ ns, $\tau_2 = 7.2$ ns, $y_0 = 0.003$ ($E_{em} = 3.44$ eV).

Thus, the time-resolved PL and PLE spectra, as well as the PL decay kinetics, point to the two relaxation processes for the CT-produced electron-hole excitations in NiO with characteristic times of nanoseconds and tens of nanoseconds, respectively. It seems quite natural to relate the two processes to types d-d and p-d CT transitions, respectively.

C. PL spectra of NiO and solid solution $Ni_xZn_{1-x}O$ under XUV excitation

The XUV excitation is believed to stimulate the bulk luminescence, mirroring the fundamental material properties, while the UV photoexcitation in NiO at $E_{exc} \geqslant E_g$ stimulates thin surface layers whose irregularities give rise to a strongly enhanced and inhomogeneously broadened luminescence. The survey luminescence spectra of the cellulose-coated NiO sample, under the XUV excitation with energy $E_{exc} = 130$ eV, are presented in Fig. 6 for the fast and slow window openings. The XUV excited luminescence for the fast window opening 100 ps after the excitation impulse starts reveals a puzzling spectral feature with two close and very narrow lines, I_1 and I_2, with a short decay time $\tau < 400$ ps peaked for the NiO sample at 3.310 eV (linewidth 17 meV) and 3.369 eV (linewidth 13 meV), respectively, mounted on a weak, broad, structureless pedestal in the 2.5–4 eV range, which is actually observed only for the slow window. It should be emphasized that the slow window spectra do not reveal any traces of the I_1-I_2 doublet.

In Fig. 7 both the I_1 and I_2 lines are shown for the fast window in more detail. To the best of our knowledge, such an unusual luminescence has not been observed to date either in NiO or other $3d$ oxides. On the other hand, the well-isolated I_1-I_2 doublet in the XUV excited luminescence seems to be a close relative of the broad high-energy (violet) band in the PL spectra peaked near 3.2 eV.

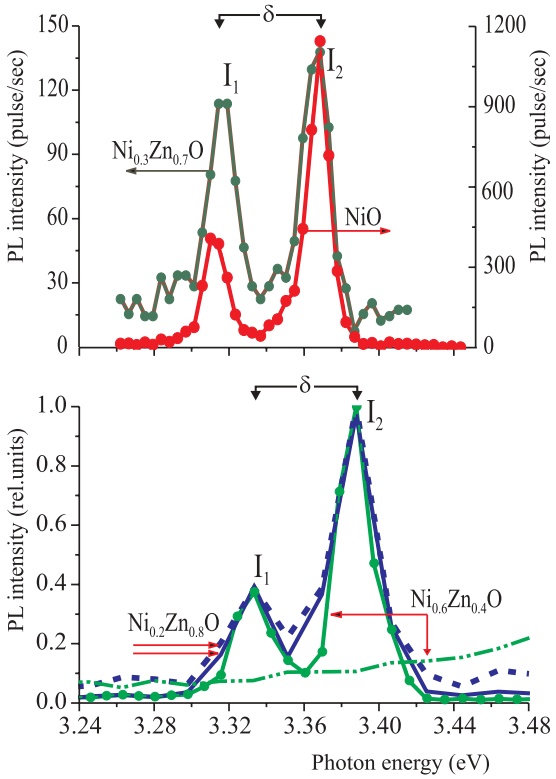

FIG. 7. (Color online) XUV excited luminescence spectra of NiO and solid solution $Ni_xZn_{1-x}O$ (fast window, spectral resolution of 10 meV). (top) Luminescence spectra of the cellulose-coated NiO and $Ni_{0.3}Zn_{0.7}O$ samples under XUV excitation with energy $E_{exc} = 130$ eV at $T = 7.2$ K. (bottom) Low-temperature ($T = 7.5$ K) luminescence spectra of the $Ni_{0.2}Zn_{0.8}O$ and $Ni_{0.6}Zn_{0.4}O$ cellulose-free samples under XUV excitation with energy $E_{exc} = 130$ eV (solid line) and $E_{exc} = 450$ eV (dashed line). Luminescence spectra of $Ni_{0.6}Zn_{0.4}O$ under XUV excitation with energy $E_{exc} = 130$ eV at $T = 7.2$ K (solid line) and room temperature (dash-dotted line).

To examine the origin of the unconventional I_1-I_2 doublet and make more reasonable suggestions about its nature, we have measured the XUV excited luminescence for the solid solution $Ni_{0.3}Zn_{0.7}O$. As in NiO we observed the I_1-I_2 doublet only for the fast window with the same energies and close linewidths (see the top panel in Fig. 7). However, the integral intensity of the I_1-I_2 doublet in $Ni_{0.3}Zn_{0.7}O$ appeared to be almost ten times weaker than in NiO, which points to the relation of the I_1-I_2 doublet with an emission produced by somehow coupled pairs of Ni ions. To exclude a conceivable parasitic effect of the cellulose coating we have measured the XUV excited luminescence for the cellulose-free ceramic samples of the solid solution $Ni_{0.2}Zn_{0.8}O$ and $Ni_{0.6}Zn_{0.4}O$ (Fig. 7, bottom panel). For the both samples we have observed the same I_1-I_2 doublet structure of the luminescence spectra with practically the same energy separation, $\delta \approx 60$ meV, and a small (20 meV) blue shift compared with the CMC-coated NiO and $Ni_{0.3}Zn_{0.7}O$ samples. Such a shift is believed to arise most likely from small strains induced by the CMC coatings. Interestingly, the novel luminescence is clearly visible only at low temperatures: the room-temperature measurements do not reveal a noticeable effect (see the room-temperature spectrum for $Ni_{0.6}Zn_{0.4}O$ in Fig. 7, which is typical for other samples). As it is seen in Fig. 7 (bottom panel) the XUV excitation with a higher energy $E_{exc} = 450$ eV does induce nearly the same I_1-I_2 doublet structure of the luminescence spectra. Thus, the unconventional soft x-ray excited violet luminescence appears to be an intrinsic property of the Ni sublattice in NiO and solid solution $Ni_xZn_{1-x}O$. Furthermore, it seems we can take the I_1-I_2 doublet to be a genuine portrait of a bulk violet luminescence free from the surface-induced defects.

III. DISCUSSION

A. *p-d* and *d-d* CT transitions in NiO

For a more comprehensive discussion of the PL and PLE effects in NiO under the VUV and XUV excitations, it will be instructive to analyze the strongest low-energy electron-hole charge-transfer transitions. The nature of radiative and nonradiative transitions in the strongly correlated $3d$ oxides is far from full understanding. However, some reliable semi-quantitative predictions can be made in the frames of a simple cluster model approach (see, e.g., Ref. 24 and references therein). The method provides a clear physical picture of the complex electronic structure and the energy spectrum, as well as the possibility of a quantitative modeling. In a certain sense the cluster calculations might provide a better description of the overall electronic structure of insulating $3d$ oxides than the band structure calculations, mainly due to a better account of correlation effects. Starting with an octahedral NiO_6 complex with the point symmetry group O_h, we deal with 5 Ni $3d$ and 18 oxygen O $2p$ atomic orbitals forming both the hybrid Ni $3d$–O $2p$ bonding and antibonding e_g and t_{2g} molecular orbitals (MO) and the purely oxygen nonbonding $a_{1g}(\sigma)$, $t_{1g}(\pi)$, $t_{1u}(\sigma)$, $t_{1u}(\pi)$, and $t_{2u}(\pi)$ orbitals. The nonbonding $t_{1u}(\sigma)$ and $t_{1u}(\pi)$ orbitals with the same symmetry are hybridized due to the oxygen-oxygen $2p\pi$–$2p\pi$ transfer. The relative energy position of different nonbonding oxygen orbitals is of primary importance for the spectroscopy of the oxygen-$3d$-metal charge transfer. This is first determined by the bare energy separation $\Delta\epsilon_{2p\pi\sigma} = \epsilon_{2p\pi} - \epsilon_{2p\sigma}$ between O $2p\pi$ and O $2p\sigma$ electrons. Since the O $2p\sigma$ orbital points towards the two neighboring positive $3d$ ions, an electron in this orbital has its energy lowered by the Madelung potential compared with the O $2p\pi$ orbitals, which are oriented perpendicular to the respective $3d$-O-$3d$ axes. Thus, the Coulomb arguments favor the positive sign of the π-σ separation $\epsilon_{p\pi}$-$\epsilon_{p\sigma}$, whose numerical value can be easily estimated in the frames of the well-known point charge model and appears to be of the order of 1.0 eV. In a first approximation, the $\gamma(\pi)$ states $t_{1g}(\pi)$, $t_{1u}(\pi)$, and $t_{2u}(\pi)$ have the same energy. However, the O $2p\pi$–O $2p\pi$ transfer and overlap yield the energy correction to the bare energies with the largest value and a positive sign for the $t_{1g}(\pi)$ state. The energy of the $t_{1u}(\pi)$ state drops due to a hybridization with the cation $4p$ $t_{1u}(\pi)$ state.

The ground state of the NiO_6^{10-} cluster, or nominally a Ni^{2+} ion, corresponds to the $t_{2g}^6e_g^2$ configuration with the Hund $^3A_{2g}(F)$ ground term. Typically, for the octahedral MeO_6 clusters[24] the nonbonding $t_{1g}(\pi)$ oxygen orbital has the highest energy and forms the first electron removal oxygen state, while the other nonbonding oxygen π orbitals, $t_{2u}(\pi)$, $t_{1u}(\pi)$, and the σ orbital $t_{1u}(\sigma)$ have a lower energy with an energy separation of $\sim$1 eV in between (see Fig. 1).

The p-d CT transition in the NiO_6^{10-} center is related to the transfer of an O $2p$ electron to the partially filled $3de_g$ subshell with the formation on the Ni site of the $(t_{2g}^6e_g^3)$ configuration of a nominal Ni^+ ion isoelectronic to the well-known Jahn-Teller Cu^{2+} ion. Yet, instead of a single p-d CT transition, we arrive at a series of O $2p\gamma \rightarrow$ Ni $3de_g$ CT transitions forming a complex p-d CT band. It should be noted that each single-electron $\gamma \rightarrow e_g$ p-d CT transition starting with the oxygen γ orbital gives rise to several many-electron CT states. For $\gamma = t_{1,2}$ these are the singlet and triplet terms $^{1,3}T_1$ and $^{1,3}T_2$ for the configurations $t_{2g}^6e_g^3\underline{t}_{1,2}$, where $\underline{t}_{1,2}$ denotes the oxygen hole. The complex p-d CT band starts with the dipole-forbidden $t_{1g}(\pi)\rightarrow e_g$, or $^3A_{2g} \rightarrow {}^{1,3}T_{1g}$, $^{1,3}T_{2g}$ transitions and then includes two formally dipole-allowed transitions, the so-called $\pi \rightarrow \sigma$ p-d CT transitions, the weak $t_{2u}(\pi)\rightarrow e_g$ and relatively strong $t_{1u}(\pi)\rightarrow e_g$ CT transitions, each giving rise to $^3A_{2g}\rightarrow {}^3T_{2u}$ transitions. Finally, the main p-d CT band is ended by the strongest dipole-allowed $\sigma \rightarrow \sigma$ $t_{1u}(\sigma) \rightarrow e_g$ ($^3A_{2g}\rightarrow {}^3T_{2u}$) CT transition. The above estimates predict the separation between the partial p-d bands to be $\sim$1 eV. Thus, if the most intense CT band, with a maximum around 7 eV, observed in the RIXS spectra[4,11,13] is attributed to the strongest dipole-allowed O $2pt_{1u}(\sigma) \rightarrow$ Ni $3de_g$ CT transition, then one should expect the low-energy p-d CT counterparts to have maxima around 4, 5, and 6 eV respectively, which are related to the dipole-forbidden $t_{1g}(\pi)\rightarrow e_g$, the weak dipole-allowed $t_{2u}(\pi)\rightarrow e_g$, and relatively strong dipole-allowed $t_{1u}(\pi)\rightarrow e_g$ CT transitions, respectively (see Fig. 1). It is worth noting that the $\pi \rightarrow \sigma$ p-d CT $t_{1u}(\pi)$-e_g transition borrows a portion of the intensity from the strongest dipole-allowed $\sigma\rightarrow\sigma$ $t_{1u}(\sigma)\rightarrow e_g$ CT transition because the $t_{1u}(\pi)$ and $t_{1u}(\sigma)$ states of the same symmetry are partly hybridized due to the p-p covalency and overlap.

Thus, the overall width of the p-d CT bands with the final $t_{2g}^6e_g^3$ configuration occupies a spectral range from $\sim$4 up to

~7 eV. The left-hand side of Fig. 1 summarizes the main semiquantitative results of the cluster model predictions for the energy and relative intensities of the p-d CT transitions. Interestingly, this assignment finds strong support in the reflectance (4.9, 6.1, and 7.2 eV for the allowed p-d CT transitions) spectra of NiO.[22] A rather strong $p(\pi)$-d CT band peaked at 6.3 eV is clearly visible in the absorption spectra of MgO:Ni.[15] The electroreflectance spectra[23] which detect the dipole-forbidden transitions clearly point to a low-energy forbidden transition peaked near 3.7 eV missed in the reflectance and absorption spectra,[12,15,22] which thus defines a p-d character of the optical CT gap and can be related to the onset transition for the whole complex p-d CT band. It should be noted that a peak near 3.8 eV has been also observed in the nonlinear absorption spectra of NiO.[25] At variance with the bulk NiO, a clearly visible intense CT peak near 3.6–3.7 eV has been observed in the absorption spectra of NiO nanoparticles.[8,26] This strongly supports the conclusion that the 3.7-eV band is related to the bulk-forbidden CT transition, which becomes the allowed one in the nanocrystalline state. It is worth noting that the hole-type photoconductivity threshold in bulk NiO has been observed also at this "magic" energy 3.7 eV;[3] that is, the $t_{1g}(\pi)\rightarrow e_g$ p-d CT transition is believed to produce itinerant holes. As a result of the p-d CT transition, a photogenerated electron localizes on a Ni^{2+} ion, forming the Jahn-Teller $3d^9$, or Ni^{1+} configuration, while a photogenerated hole can move more or less itinerantly in the O $2p$ valence band determining the holelike photoconductivity.[3] It should be noted that any oxygen π holes have a larger effective mass than the σ holes, which results in different roles for the $p(\pi)$-d and $p(\sigma)$-d CT transitions, both in photoconductivity[27] and, probably, in the luminescence stimulation.

Indeed, turning back to our PLE spectra (Fig. 4), we can now certainly attribute the spectral feature near 6 eV, clearly visible for both the CMC-free and CMC-coated NiO samples, to a rather strong $p(\pi)$-d $[t_{1u}(\pi) \rightarrow e_g]$ CT transition, while the spectral feature near 5 eV, particularly clearly visible for the CMC-free NiO sample, are attributable to the weaker $p(\pi)$-d $[t_{2u}(\pi) \rightarrow e_g]$ CT transition. Interestingly, the strongest $p(\sigma)$-d $[t_{1u}(\sigma) \rightarrow e_g]$ CT transition at ~7 eV is actually inactive in the PL excitation, most likely due to a dominating nonradiative relaxation channel for the oxygen $t_{1u}(\sigma)$ holes.

The p-d CT model cannot explain the main low-energy feature in the PLE spectra near 4 eV, which is clearly visible for both the CMC-free and CMC-coated NiO samples (Fig. 4). However, along with the p-d CT transitions an important contribution to the optical response of the strongly correlated $3d$ oxides can be related to the strong dipole-allowed d-d CT, or Mott transitions.[24] In NiO one expects a strong d-d CT transition related to the σ-σ-type e_g-e_g charge transfer $t_{2g}^6e_g^2 + t_{2g}^6e_g^2 \rightarrow t_{2g}^6e_g^3 + t_{2g}^6e_g^1$ between nnn Ni sites with the creation of electron NiO_6^{11-} and hole NiO_6^{9-} centers (nominally, Ni^+ and Ni^{3+} ions, respectively), thus forming a bound electron-hole dimer, or d-d CT exciton. The charge, spin, and orbital degeneracy of the final state of this unique double anti-Jahn-Teller transition $^3A_{2g} + {}^3A_{2g} \rightarrow {}^2E_g + {}^2E_g$ results in its complex structure. The exchange tunnel reaction $Ni^+ + Ni^{3+} \leftrightarrow Ni^{3+} + Ni^+$ due to a two-electron transfer gives rise to the two symmetric (S and P) excitons (see Fig. 8) having s and p symmetry, respectively, with energy

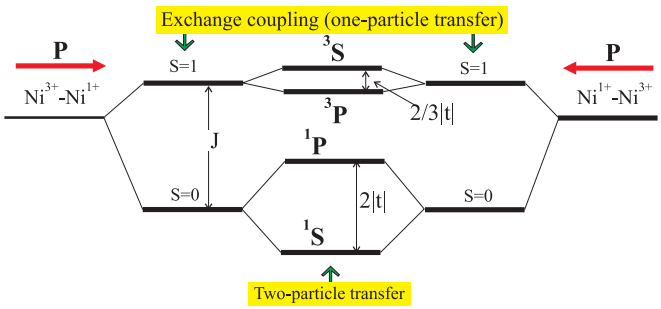

FIG. 8. (Color online) Illustration of the formation of spin-singlet and spin-triplet S- and P-type d-d CT excitons in NiO. Arrows point to the orientation of the electric dipole moment.

separation $\delta_0 = 2|t|$ and $\delta_1 = \frac{2}{3}|t|$ for the spin singlet and spin triplet excitons, where t is the two-electron transfer integral whose magnitude is of the order of the Ni^{2+}-Ni^{2+} exchange integral:[28] $t \approx I_{nnn}$. Interestingly, the P exciton is dipole allowed, while the S exciton is dipole forbidden. The strong dipole-allowed Franck-Condon $d(e_g)$-$d(e_g)$ CT transition in NiO manifests itself as a strong spectral feature near 4.5 eV that is clearly visible in the absorption of the thin NiO films,[14] RIXS spectra,[4,13] and the reflectance spectra (4.3 eV).[22] Such a strong absorption near 4.5 eV is beyond the predictions of the p-d CT model and indeed is lacking in the absorption spectra of MgO:Ni.[15] It should be noticed that, unlike all the above-mentioned structureless spectra, the nonlinear absorption spectra[25] of NiO films do reveal an anticipated "fine" structure of the d-d CT exciton with the two narrow peaks at 4.075 and 4.33 eV preceding a strong absorption above 4.575 eV. Interestingly, the separation 0.2–0.3 eV between the peaks is typical for the exchange-induced splittings in NiO (see, e.g., the "0.24 eV" optical feature[12]).

Accordingly, the 4.1-eV peak in the PLE spectra (see Fig. 4) can be unambiguously assigned to the d-d CT transition. Furthermore, we argue that such a transition is believed to be a main contributor to the fast window, the high-energy violet component of the PL spectra.

B. d-d CT luminescence in NiO

As usual, for different $3d$ compounds the UV excited red and green luminescences in NiO are related to different d-d crystal-field transitions.[7–10] What is the origin of the unconventional x-ray excited violet luminescence regularly observed for NiO and solid solution $Ni_xZn_{1-x}O$? There are three types of candidate initial states for the proper radiative transition: (i) the excited $^1T_{1g}(G)$ or $^1A_{1g}(G)$ terms of $(3d^8)Ni^{2+}$ configuration, whose Franck-Condon energies were found by Newman and Chrenko[12] as 3.52 and 3.25 eV, respectively, (ii) the self-trapped p-d $[t_{1g}(\pi)\rightarrow e_g]$ CT exciton, and (iii) the self-trapped d-d $(e_g\rightarrow e_g)$ CT exciton.

Several arguments rule out the d-d crystal-field transitions $^1T_{1g}(G)$, $^1A_{1g}(G)\rightarrow {}^3A_{2g}(F)$ as a source of an unconventional x-ray excited luminescence. First, the excited $^1T_{1g}(G)$ and $^1A_{1g}(G)$ terms can nonradiatively relax to the close low-lying terms $^3T_{1g}(P)$ and $^1T_{2g}(D)$. Second, typically, the radiative crystal-field transitions produce broad luminescence bands with long lifetimes.[7]

The situation seems to be more obscure with the self-trapping and radiative deexcitation of the *p-d* and *d-d* CT excitons. The *p-d* CT excitons have been observed in some impure II-VI:3*d* compounds as narrow lines preceding broad intense *p-d* CT absorption bands.[29] However, to the best of our knowledge, there are no reliable literature data regarding the observation of the self-trapping for *d-d* CT excitons. Most likely, the CT excitons have not been observed in photoluminescence mainly due to nonradiative transitions to intracenter 3*d* states; hence the *d-d* crystal-field transitions are usually addressed as the main contributors to photoluminescence in 3*d* compounds.

The observation of green luminescence in ZnO:Cu with a sharp zero-phonon line at 2.859 eV (Ref. 30) is perhaps the only reliable evidence of the self-trapping and radiative deexcitation of the *p-d* CT exciton. The uniqueness of ZnO:Cu is that the radiative *p-d* CT transition is well isolated from the only crystal-field $3d^9{:}^2E \rightarrow 3d^9{:}^2T_2$ transition by the energy gap of almost 2 eV that blocks the nonradiative deexcitation of the CT state. Interestingly, a similar situation with the observation of the ligand-cation CT luminescence is realized in a large body of compounds with the rare-earth Yb^{3+} ion.[31]

However, the low-lying *p-d* $[t_{1g}(\pi) \rightarrow e_g]$ CT excitonic states are not likely responsible for the violet luminescence in NiO. Indeed, instead of the rather weak *p-d* CT excitation channel of the $\pi \rightarrow \sigma$ type the most effective channel of the recombinational relaxation for the spin-triplet *p-d* CT states $t_{2g}^6 e_g^3 \underline{\gamma}(\pi)$ $[\gamma(\pi) = t_{1g}(\pi), t_{2u}(\pi), t_{1u}(\pi)]$ in NiO implies the stronger $\pi \rightarrow \pi$ transfer $t_{2g} \rightarrow \gamma(\pi)$ with the formation of excited spin-triplet $^3T_{1g}$ or $^3T_{2g}$ states of the $t_{2g}^5 e_g^3$ configuration of the Ni^{2+} ion. This nonradiative Auger recombination (nAR)[33] is followed by a final relaxation to the lowest singlet terms, $^1T_{2g}$ and ^1E_g, producing the green and red luminescences, respectively. Obviously, this relaxation is strongly enhanced by any symmetry-breaking effects lifting or weakening the selection rules. The *p-d* CT excitation-relaxation sequence can be represented as follows (see Ref. 33):

$$[Ni^{2+}O_6]_{GS} \overset{p-dCT}{\longrightarrow} [Ni^{+}O_6]^* \rightarrow [Ni^{+}O_6]_{GS} \overset{nAR}{\rightarrow} [Ni^{2+}O_6]^* \longrightarrow [Ni^{2+}O_6]_{GS}. \quad (1)$$

Thus, the three $\pi \rightarrow \sigma$ *p-d* CT transitions are $t_{1g}(\pi) \rightarrow e_g$, $t_{2u}(\pi) \rightarrow e_g$, and $t_{1u}(\pi) \rightarrow (e_g$ in NiO are expected to effectively stimulate the green luminescence). However, these transitions cannot explain the origin of the violet luminescence, in particular, the specific I_1-I_2 doublet stimulated by the XUV excitation, whose concentration behavior points to participation of Ni pairs, or *d-d* CT transitions rather than the isolated NiO_6 centers. Indeed, it seems the unique "double" Jahn-Teller *d-d* CT exciton $t_{2g}^6 e_g^3; {}^2E_g + t_{2g}^6 e_g^1; {}^2E_g$ self-trapped in the lattice due to the electron-hole attraction and strong Jahn-Teller coupling with a reasonable Stokes shift of ~1 eV remains the only candidate for producing the unconventional x-ray excited luminescence. In such a case the I_1-I_2 doublet can be a Stokes shifted radiative counterpart of the X_2-X_3 excitonic states observed in nonlinear optical absorption spectra of NiO films[25](see Fig. 8). It is worth noting that different optical reflectance and absorption measurements[12,22,32] have not as yet revealed any spectral features near 3.3 eV, which could be related to the self-trapped *d-d* CT exciton. Interestingly, the I_1-I_2 separation ($\delta \approx 60$ meV) agrees with the theoretically predicted $\delta_{tun} \approx 2|I_{nnn}| \sim 70$ meV if we make use of the estimates for I_{nnn} in Ref. 1. The narrowness of the I_1 and I_2 lines underlines the extremely localized character of the double Jahn-Teller *d-d* CT exciton.

Strictly speaking, the *d-d* CT excitation-relaxation sequence we have addressed above can be represented as follows:

$$[d^8 - d^8] \overset{d-dCT}{\longrightarrow} [d^9 - d^{7*}] \rightarrow [d^9 - d^{7*}]_{STE} \overset{I_{1,2}}{\longrightarrow} [d^8 - d^8], \quad (2)$$

where the first step implies the Franck-Condon *d-d* CT transition with the final low-spin $t_{2g}^6 e_g^1{:}^2E_g$ state of the Ni^{3+} ion, which appears to be an excited state with $3d^7$ configuration ($3d^{7*}$) separated from the high-spin $t_{2g}^5 e_g^2{:}^4T_{1g}$ ground state by an energy gap of ~1.0 eV given $Dq \approx 0.1$ eV.[12] Hence we should consider two alternative complementary relaxation channels for the $[d^9 - d^{7*}]$ CT state with the on-site $3d^{7*} \rightarrow 3d^7$ $(t_{2g}^6 e_g^1 : {}^2E_g \rightarrow t_{2g}^5 e_g^2 : {}^4T_{1g})$ transformation:

$$[d^9 - d^{7*}] \rightarrow [d^9 - d^7] \overset{AR}{\longrightarrow} [d^8 - d^{8*}] \longrightarrow [d^8 - d^8] \quad (3)$$

and

$$[d^9 - d^{7*}] \rightarrow [d^9 - d^7] \rightarrow [d^9 - d^7]_{STE} \rightarrow [d^8 - d^8]. \quad (4)$$

The first channel implies a middle Auger recombination process: $t_{2g}^6 e_g^3; {}^2E_g + t_{2g}^5 e_g^2; {}^4T_{1g} \rightarrow t_{2g}^6 e_g^2; {}^3A_{2g} + t_{2g}^5 e_g^3; {}^3T_{2g}$ due to a dipole-allowed $\sigma \rightarrow \sigma$ *d-d* CT transition to a final Ni^{2+}-Ni^{2+} configuration with one of the ions in the excited $t_{2g}^5 e_g^3; {}^3T_{2g}$ state. Interestingly, the last two steps in this sequence with energies $E_{AR} \approx 2.5$ eV and $E[{}^3T_{2g}(F)] \approx 1.0$ eV, respectively, could be related to radiative transitions in green and near infrared bands.

The second channel implies a self-trapping of the $[d^9 - d^7]$ *d-d* CT exciton with energy $E_{STE} \leqslant 3.0$ eV, whose reasonable estimation assumes a Jahn-Teller stabilization energy of $E_{JT} \geqslant 0.5$ eV. The recombination transition $[d^9 - d^7] \rightarrow [d^8 - d^8]$ is dipole forbidden; however, a near degeneracy with several excited $3d^8$ terms points to the feasibility of a nonradiative energy transfer to the on-site Ni^{2+} excitations. It should be noted that the on-site transformation $t_{2g}^6 e_g^1; {}^2E_g \rightarrow t_{2g}^5 e_g^2; {}^4T_{1g}$ of the Ni^{3+} center implies the configurational change that strongly suppresses the potency of the both channels. Nevertheless, the nonradiative transition of the double Jahn-Teller $[d^9 - d^{7*}]$ $(t_{2g}^6 e_g^3; {}^2E_g + t_{2g}^6 e_g^1; {}^2E_g)$ CT exciton self-trapped in the lattice to a nearby $[d^9 - d^7]$ CT excitonic state could be one of the contributors to a temperature quenching of the I_1-I_2 luminescence.

It is worth noting that the self-trapped *d-d* excitons can be formed also due to a trapping of the oxygen hole as a result of the *p-d* CT transition on the nearest Ni^{2+} ion. Furthermore, the excitation of the $t_{2g}^6 e_g^3 \underline{t}_{1g}(\pi)$ *p-d* CT exciton at an energy of 3.7–3.8 eV, which is sizeably below the energy of the strongest *d-d* CT transition at 4.5 eV, can efficiently stimulate the violet luminescence due to a self-trapping of the oxygen $t_{1g}(\pi)$ hole in the t_{2g} orbital on the adjacent Ni^{2+} ion.

The dramatic difference in the violet luminescence spectra under the XUV and VUV excitations seems to be explained

if we account for different attenuation lengths of the VUV and XUV quanta. The x-ray attenuation length for NiO is given as 30 nm at 130 eV and 225 nm at 450 eV,[34] with the first value being not very different from the value of $\leqslant$20 nm typical for the VUV excitation in NiO. Strictly speaking, we should consider all relevant factors, including, but not limited to, the attenuation length. Among other factors worth noting is the significantly larger excitation energy of the XUV compared to VUV quanta. The Ni^{2+} on-site high-energy interconfigurational transitions imply excitations to final spatially extended electron states which are prone to the intersite d-d rather than d-p charge transfer. In other words, the relaxation sequence of the Ni^{2+} on-site high-energy electronic excitations implies an enhanced concentration of $[d^{7*} - d^{9*}]$ states with a final self-trapping and I_1-I_2 d-d CT recombination luminescence.

IV. CONCLUSION

The luminescence spectra of NiO and solid solution $Ni_xZn_{1-x}O$ with the rock-salt-type structure have been investigated under VUV excitation in the wide spectral range 4–12 eV and XUV excitation with two excitation energies (130 and 450 eV). The PL spectra show broad emission green and violet bands centered at about 2.3 and 3.2 eV, respectively. The PL spectral evolution and lifetime measurements under VUV excitation reveal that two mechanisms with long and short decay times, respectively, are responsible for the observed emissions. These mechanisms are related to $p(\pi)$-d and d-d CT transitions in the range 4–6 eV. The $d(e_g)$-$d(e_g)$ CT transition peaked near 4 eV is believed to be the most effective one in the excitation of the high-energy violet part of the PL spectrum. Making use of the PLE spectra recorded in the 4–7 eV range, we succeeded in distinctly separating contributions of $p(\pi)$-d, $p(\sigma)$-d, and d-d CT transitions into the optical response of NiO. The PL and PLE spectroscopies are shown to provide an instructive tool to elucidate the mechanism of the charge transfer in strongly correlated 3d oxides.

A soft x-ray excitation makes it possible to avoid a predominant role of the surface effects in luminescence and reveals a bulk violet luminescence with the puzzling well-isolated I_1-I_2 doublet with very narrow lines with close energies near 3.3 eV in both NiO and solid solution $Ni_xZn_{1-x}O$. A comparative analysis of the p-d and d-d CT transitions, their relaxation channels, and luminescence spectra for NiO and $Ni_{0.3}Zn_{0.7}O$ points to a recombination transition in self-trapped nnn Ni^{+}-Ni^{3+} d-d CT excitons as the only candidate source for the unconventional luminescence. Thus we can address the I_1-I_2 doublet as a genuine portrait of the bulk violet luminescence free from the surface-induced defects. The cellulose coating of the NiO samples resulted in a spectacular growth of the PL intensities and the signal-to-noise ratio, pointing to a specific role of the surface effects under the VUV excitation. However, the persistent observation of the I_1-I_2 doublet luminescence under the XUV excitation in both the cellulose-coated and cellulose-free samples of NiO and $Ni_xZn_{1-x}O$ provides strong evidence that the effect has an intrinsic bulk nature.

The appearance of the unconventional d-d CT luminescence is feasible only under specific conditions. The uniqueness of NiO is that the d-d CT exciton formed by the anti-Jahn-Teller transition $^3A_{2g} + {}^3A_{2g} \rightarrow {}^2E_g + {}^2E_g$ in Ni^{2+}-Ni^{2+} pairs is prone to be self-trapped in the lattice due to the electron-hole attraction and a particularly strong double Jahn-Teller effect for both the electron and hole centers. A more explicit assignment of I_1 and I_2 lines requires further detailed analysis of the electron-lattice, spin-orbital, and exchange coupling effects together with additional measurements of the temperature and external field effects at different excitation energies.

We have presented a comprehensive cluster model description of the p-d and d-d CT transitions in NiO. We argue that the CT gap in NiO is formed by a superposition of the electrodipole forbidden p-d $[t_{1g}(\pi) \rightarrow e_g]$ and allowed $d(e_g)$-$d(e_g)$ CT transitions with close energies. In fact, the prototype 3d oxide NiO, similar to perovskite manganites $RMnO_3$ or parent cuprates such as La_2CuO_4,[24] should instead not be sorted into either the CT insulator or the Mott-Hubbard insulator in the Zaanen-Sawatzky-Allen scheme.[5]

ACKNOWLEDGMENTS

The authors are grateful to R. V. Pisarev, V. I. Anisimov, and A. V. Lukoyanov for discussions. Portions of this research were carried out at the HASYLAB (DESY), Projects No. II-20080019 and No. I-20110050 (SUPERLUMI station, beamline I). We would like to thank M. Kirm, Anthony M. T. Bell, and Edmund Welter for help with the BW3, B2, and A1 experiments. Anthony M. T. Bell and V. Guzikova are gratefully acknowledged for corrections to the English. This work was partially supported by the Ural Branch of RAS (Grant No. 12-U-2-1030) and RFBR Grants No. 10-02-96032 and No. 12-02-01039 (A.S.M.).

[1] B. Brandow, Adv. Phys. **26**, 651 (1977); S. Hüfner, *ibid.* **43**, 183 (1994).

[2] J. Wu, C.-W. Nan, Y. Lin, and Y. Deng, Phys. Rev. Lett. **89**, 217601 (2002); H. Shima, F. Takano, H. Akinaga, Y. Tamai, I. H. Inoue, and H. Takagi, Appl. Phys. Lett. **91**, 012901 (2007); H. Ohldag, A. Scholl, F. Nolting, E. Arenholz, S. Maat, A. T. Young, M. Carey, and J. Stöhr, Phys. Rev. Lett. **91**, 017203 (2003).

[3] Ya. M. Ksendzov and I. A. Drabkin, Fiz. Tverd. Tela **7**, 1884 (1965) [Soviet Phys. Solid State **7**, 1519 (1965)].

[4] N. Hiraoka, H. Okamura, H. Ishii, I. Jarrige, K. D. Tsuei, and Y. Q. Cai, Eur. Phys. J. B **70**, 157 (2009).

[5] J. Zaanen, G. A. Sawatzky, and J. W. Allen, Phys. Rev. Lett. **55**, 418 (1985).

[6] K. S. Song and R. T. Williams, *Self-Trapped Excitons* (Springer, Berlin, 1993).

[7] C. Díaz-Guerra, A. Remón, J. A. García, and J. Piqueras, Phys. Status Solidi A **163**, 497 (1997).

[8] V. V. Volkov, Z. L. Wang, and B. S. Zou, Chem. Phys. Lett. **337**, 117 (2001).

[9] S. Mochizuki and T. Saito, Phys. B **404**, 4850 (2009).
[10] A. Kuzmin, N. Mironova-Ulmane, and S. Ronchin, Proc. SPIE **5122**, 61 (2003).
[11] M. Magnuson, S. M. Butorin, A. Agui, and J. Nordgren, J. Phys. Condens. Matter **14**, 3669 (2002).
[12] R. Newman and R. M. Chrenko, Phys. Rev. **114**, 1507 (1959).
[13] L.-C. Duda, T. Schmitt, M. Magnuson, J. Forsberg, A. Olsson, J. Nordgren, K. Okada, and A. Kotani, Phys. Rev. Lett. **96**, 067402 (2006); B. C. Larson, J. Z. Tischler, W. Ku, C. C. Lee, O. D. Restrepo, A. G. Eguiluz, P. Zschack, and K. D. Finkelstein, *ibid.* **99**, 026401 (2007).
[14] C. E. Rossi and W. Paul, J. Phys. Chem. Solids **30**, 2295 (1969).
[15] K. W. Blazey, Phys. B **89**, 47 (1977).
[16] A. N. Baranov, P. S. Sokolov, O. O. Kurakevich, V. A. Tafeenko, D. Trots, and V. L. Solozhenko, High Press. Res. **28**, 515 (2008).
[17] M. Knapp, C. Baehtz, H. Ehrenberg, and H. Fuess, J. Synchrotron Radiat. **11**, 328 (2004).
[18] M. Knapp, V. Joco, C. Baehtz, H. H. Brecht, A. Berghaüser, H. Ehrenberg, H. von Seggern, and H. Fuess, Nucl. Instrum. Methods Phys. Res., Sect. A **521**, 565 (2004).
[19] L. C. Bartel and B. Morosin, Phys. Rev. B **3**, 1039 (1971).
[20] V. A. Pustovarov, V. Yu. Ivanov, V. I. Sokolov, N. B. Gruzdev, A. N. Baranov, and P. S. Sokolov, DESY, HASYLAB, Annual Report-2010, Hamburg, Germany, 20101113 (2011) (unpublished).
[21] C. S. Lao, M.-C. Park, Q. Kuang, Y. Deng, A. K. Sood, D. L. Polla, and Z. L. Wang, J. Am. Chem. Soc. **129**, 12096 (2007).
[22] R. J. Powell and W. E. Spicer, Phys. Rev. B **2**, 2182 (1970).
[23] J. L. McNatt, Phys. Rev. Lett. **23**, 915 (1969); R. Glosser and W. C. Walker, Solid State Commun. **9**, 1599 (1971).
[24] A. S. Moskvin, Phys. Rev. B **65**, 205113 (2002); R. V. Pisarev, A. S. Moskvin, A. M. Kalashnikova, and Th. Rasing, *ibid.* **79**, 235128 (2009); A. S. Moskvin and R. V. Pisarev, Low Temp. Phys. **36**, 613 (2010); A. S. Moskvin, Opt. Spectrosc. **111**, 403 (2011).
[25] S. I. Shablaev and R. V. Pisarev, Phys. Solid State **45**, 1742 (2003).
[26] S. Chakrabarty and K. Chatterjee, J. Phys. Sci. **13**, 245 (2009).
[27] Most likely, Ksendzov and Drabkin (Ref. 3) observed the $p(\pi)$ hole conductivity in a halide-decomposition NiO crystal stimulated by forbidden $p(\pi)$-d $[t_{1g}(\pi) \rightarrow e_g]$ CT transition, whereas an attempt to observe photoconductivity in flame-fusion-grown NiO crystals gave negative results up to 7 eV (Ref. 22), that is, up to the energy of allowed $p(\sigma)$-d $[t_{1g}(\sigma) \rightarrow e_g]$ CT transition stimulating the $p(\sigma)$ hole conductivity.
[28] A. S. Moskvin, Phys. Rev. B **84**, 075116 (2011).
[29] V. I. Sokolov and K. A. Kikoin, Sov. Sci. Rev. A **12**, 147 (1989); V. I. Sokolov, Fizika i Tekhnika Poluprovodnikov **28**, 545 (1994) [Semiconductors **28**, 329 (1994)].
[30] R. Dingle, Phys. Rev. Lett. **23**, 579 (1969); D. J. Robbins, J. Lumin. **24/25**, 137 (1981).
[31] L. van Pieterson, M. Heeroma, E. de Heer, and A. Meijerink, J. Lumin. **91**, 177 (2000).
[32] V. Propach, D. Reinen, H. Drenkhahn, and H. Müller-Buschlaum, Z. Naturforsch. B **33**, 619 (1978).
[33] D. J. Robbins and P. J. Dean, Adv. Phys. **27**, 499 (1978).
[34] X-ray interactions with matter, http://henke.lbl.gov/optical_constants/.